

EINDHOVEN UNIVERSITY OF TECHNOLOGY

Vision-based deposition geometry detection

Algorithm Design for Additive Manufacturing

A paper submitted in fulfilment of the requirements for the completion of the Systems and Control Master (20 ECTS) Internship Project .

The internship was performed at the University of Waterloo within the Multi-Scale Additive Manufacturing Lab in a period of 14 Weeks and 5 days between 09/01/2016 and 12/13/2016 .

Author:

G.J.J. van Houtum
IDnr: 0872274

EINDHOVEN UNIVERSITY OF TECHNOLOGY

Vision-based deposition geometry detection

Algorithm Design for Additive Manufacturing

A paper submitted in fulfilment of the requirements for the completion of the Systems and Control Master (20 ECTS) Internship Project .

The internship was performed at the University of Waterloo within the Multi-Scale Additive Manufacturing Lab in a period of 14 Weeks and 5 days between 09/01/2016 and 12/13/2016 .

Author:

G.J.J. van Houtum

IDnr: 0872274

University of Waterloo

Department of Mechanical and Mechatronics Engineering

Multi-Scale Additive Manufacturing Lab

Supervisor: M.L. Vlasea, PhD

Eindhoven University of Technology

Department of Mechanical Engineering

Control Systems Technology

Supervisor: Dr.ir. Etman

Tilburg, Netherlands, May 2018

Preface

This report is the result of the 20 week Research Internship performed at the University of Waterloo in Canada within the Multi-Scale Additive Manufacturing Lab. The internship is part of the Systems and Control Master program at Eindhoven University of Technology in the Netherlands.

The main targeted audience for this report are people interested in algorithm design for machine vision systems and people within Additive Manufacturing interested in monitoring techniques for deposition based systems.

Readers interested in hardware selection for triangulation based visual detection should take a look at Chapter 2. Design limitations of algorithm design and previous work done in the field is discussed in Chapter 3. Chapter 4 presents a new detection algorithm for detection of width and height.

I would like to give special thanks to M.L. Vlasea, PhD for her advice and supervision of the project. Furthermore i would like to thank Dr.ir. Etman for his patience, general advice and mentoring.

Abstract

Conventional manufacturing processes lack the free form capabilities additive manufacturing (AM) has. Achieving accuracy and short production time are however challenging to achieve with AM. If these problem could be resolved, AM could replace the conventional methods to mass produce more complex parts.

Feedback control of deposited material dimensions in soft material AM extrusion processes could improve the accuracy of parts. Measuring the deposition is possible using a triangulation based vision system consisting out of a camera and a laser-diode. Algorithms exist to extract geometric features such as height and width but lack flexibility and robustness against noise.

A literature review on algorithm design for triangulation based vision systems and an experimental low-quality vision system are used to identify the limitations in current algorithms and their applicability to low-quality vision hardware.

This research produces a new algorithm able to detect height and width of deposition material for additive manufacturing processes. It is able to operate under pixel saturation and inhomogeneity of the laser line. It is flexible since only one parameter is needed for the algorithm.

Contents

Preface	v
Abstract	vii
Lists	xi
Figures	xi
Tables	xi
1 Introduction	1
2 Vision System	3
2.1 Overview	3
2.2 Triangulation Configuration	4
2.3 Camera	6
2.4 Laser-Diode	7
2.5 Deposition Material	8
3 Algorithm Design Limitations	9
3.1 Objective	9
3.2 Data limitations	10
3.3 Previous Work	11
4 Proposed Algorithm	15
4.1 Overview	15
4.2 Image representation	16
4.3 Deposition Segmentation	17
4.4 Laser Line Edge Segmentation	21
4.5 Width measurement	24
4.6 Height measurement	25
5 Conclusions and Recommendations	27
Bibliography	30

Lists

Figures

2.1	Overview of vision system components.	3
2.2	Overview of vision system in reality.	4
2.3	Laser Line Triangulation	4
2.4	Dino-Lite Camera	6
2.5	Infiniter Line-Laser	7
2.6	Camera view for different types of deposition material.	8
3.1	Image from vision system with applicable terms to image sections.	10
4.1	Image channels in gray-scale and total image in RGB.	16
4.2	Template Matching of I_{rc2} with $\delta_1 = C - \delta_2 = 130$.	18
4.3	Total Error as euclidean distance of normalized sum-of-squared errors.	19
4.4	Triangle based segmentation versus differencing.	20
4.5	Triangle based thresholding versus Otsu's method.	22
4.6	Edge segmentation of the laser line on the print bed.	24
4.7	Width extraction at the position of the laser line edge.	25
4.8	Height extraction.	26

Tables

2.1	Triangulation Configuration Rankings.	5
2.2	Dino-Lite Specifications	6
2.3	Dino-Lite camera data output.	7
2.4	Laser Specifications.	7

1 Introduction

Additive Manufacturing (AM) has the ability to produce more complex products than conventional manufacturing processes. Dimensional accuracy, repeatability and short production time are however challenging to achieve within AM processes. Specifically, extrusion based additive manufacturing processes for soft materials. If the predescribed problems could be overcome AM could replace these conventional methods for mass production and save money due to its free form capabilities.

Triangulation based vision systems consisting out of a camera and a laser are often used for monitoring the printed material in real-time. This way, failure can be detected before completion of the part and the process could be stopped to save time. Accuracy could be improved if real time geometry measurements are used as sensor data for a control algorithm.

Many algorithms exist for detecting width and height of the deposition material but often rely on a lot of parameters to be tuned. Noise and disturbance in hardware components is often neglected and material properties such as reflectiveness is not accounted for.

The goal of this report is to design a robust vision-based detection algorithm able to detect feature height and width for additive manufacturing material extrusion processes. On the basis of a literature review and noisy images from a low cost experimental triangulation based vision system a new algorithm is designed. The focus of this research lies on the algorithm design. The vision system is selected to produce low quality video output to produce a noisy environment.

The hardware selection, operation, positioning and the images it outputs are discussed in Chapter 2. Chapter 3 describes the results from the literature review and data implied limitations. The new proposed algorithm is discussed in chapter 4.

2 Vision System

This research is focused on the development of an image processing algorithm able to detect deposition geometry in a robust manner. By robust is meant that the algorithm should still be able to detect the right geometry under sub-optimal image conditions. The images the algorithm processes are generated by the vision system hardware. To test robustness a vision system has been selected consisting out of low-quality components.

The vision system hardware setup is discussed in this chapter. First, an overview is given of all the elements in the vision system. Then the different triangulation configurations are discussed. Next, the major components are further explained and at last the generated output is analyzed.

2.1 Overview

A general overview of the components of the experimental setup is shown in Figure 2.1. The vision system consists out of a camera and a laser which are fixed in position by a mount bracket. This bracket is attached to the AM machine. The laser exposes the geometry of the line deposited on the bed. The camera is connected to the laptop and the software runs the image processing algorithm on the images from the camera detecting the geometry of the depositions. An overview of the vision system in reality

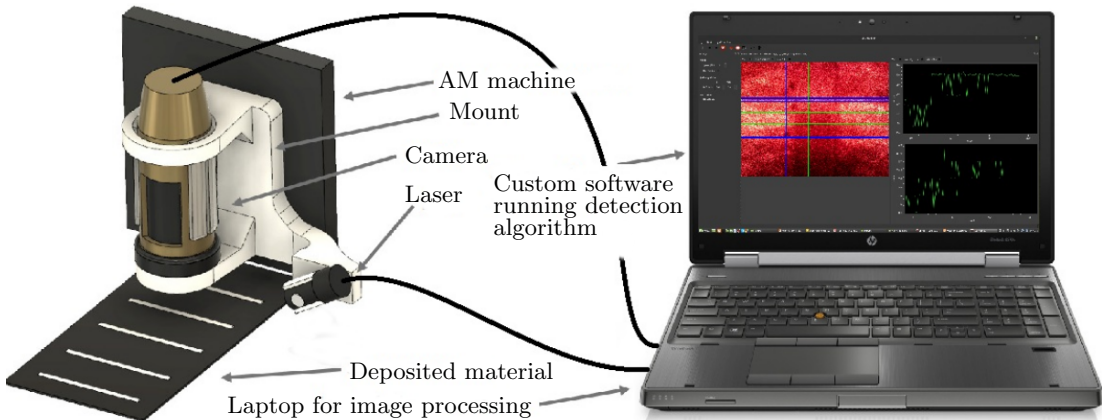


Figure 2.1: Overview of vision system components.

is shown in Figure 2.2. The laser emits a red colored line which illuminates the deposited material. The laser line quality is low as shown by the noise around the center of the line. The line follows the geometry of the deposition exposing the profile to the camera. The deposition lines are printed and UV-cured as described in [1].

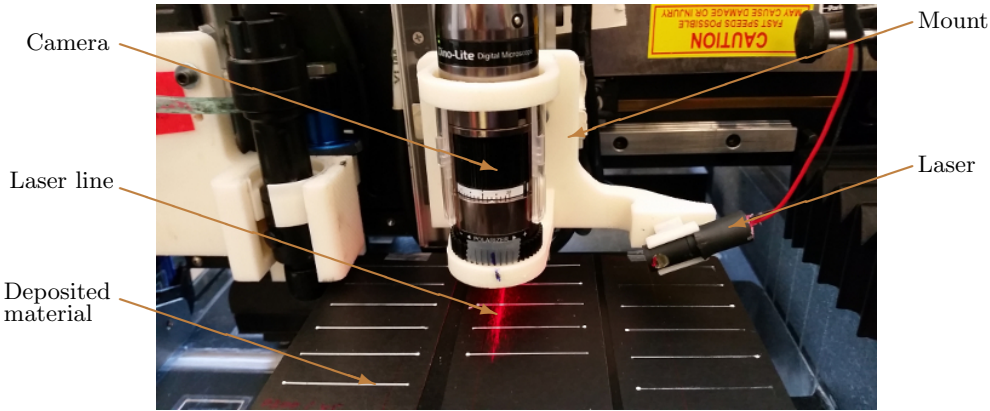


Figure 2.2: Overview of vision system in reality.

2.2 Triangulation Configuration

A triangulation based configuration is used for the measurement of the deposition geometry. This configuration consists out of a line-laser and a camera placed at a relative angle to each other. The line emitted by the laser illuminates the material in its path. A different angle of the camera relative to the laser is needed to expose the geometry of the illuminated material. Images created by the camera are generally thought to look as displayed in Figure 2.3b. The angular placement of the components with respect to each other and the bed has consequences for the quality of the images created. Four commonly used configuration setups are shown in Figure 2.3a and the side view of the reverse configuration in Figure 2.3c.

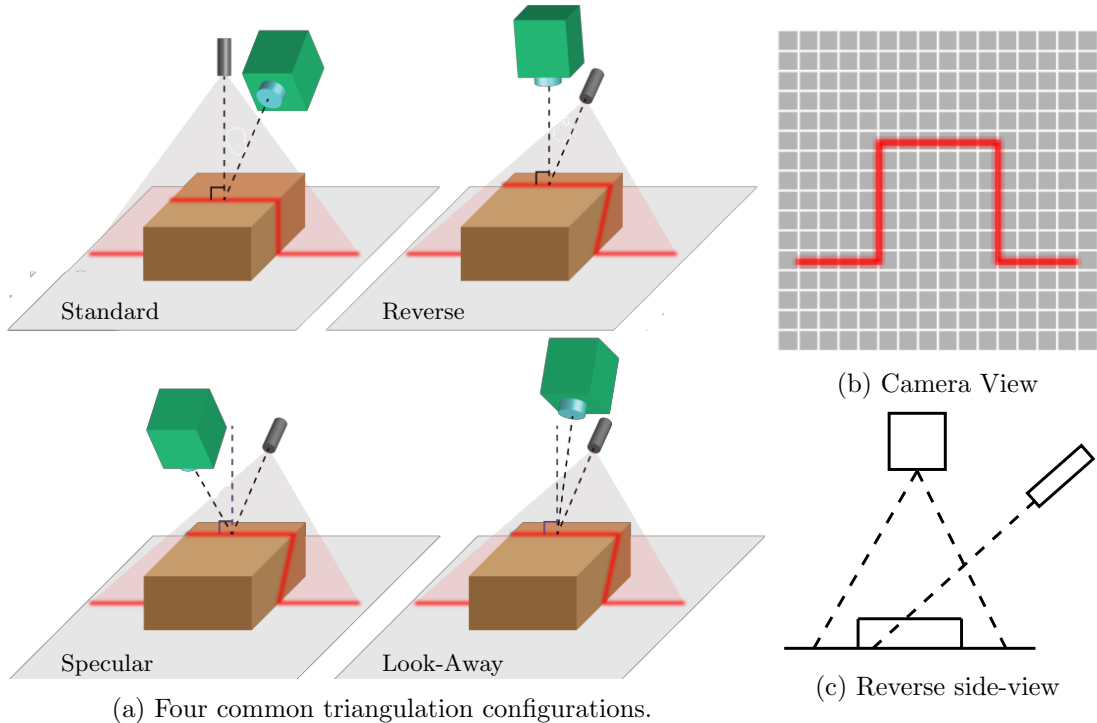


Figure 2.3: Laser Line Triangulation

Each configuration has advantages and disadvantages. Important factors to consider when choosing a configuration are:

Resolution Placing the laser at a shallow angle with respect to the bed, and the camera at 90 degrees relative to the laser is optimal for a large height resolution. The camera view as shown in Figure 2.3b would show a large line height. This is advantages for the measurement of height from the image.

Focus Placing the camera at a shallow angle with respect to the bed will result in focus loss. Only a very narrow point on the deposition will be focused. The camera at 90 degrees will be able to focus on the whole field of view and the best pixel/inch ratio. At this point the least amount of deposition area is converted to the largest amount of pixels. The shallower the angle the lower the ratio.

Line Spreading Placing the laser at a shallow angle spreads the line out over a larger area compared to an angle of 90 degrees relative to the bed. The line will therefore loose brightness.

Dimensions The larger the components the further away they should be placed. Small components can be placed very close influencing factors.

Inclusion A shallow angle for the camera or laser will result in material inclusion. The camera or laser will not be able to illuminate or observe a certain area of the material because some other material stands in the way.

Reflection Certain angles between the camera and the laser will result in reflection. The laser will then saturate the image and pixel difference will be lost.

Using the above factors the four common configurations are ranked. Table 2.1 shows the score of each configuration at each factor. The Standard and Reverse configuration

Configuration	Standard	Reverse	Specular	Look-Away
Resolution	+	++	+++	-
Focus	-	+++	+	++
Line Spreading	+++	-	++	+
Dimensions	+	++	+++	-
Inclusion	++	+	-	+++
Reflection	++	+	-	+++
Score	8	8	7	7

Table 2.1: Triangulation Configuration Rankings.

score best. Each configuration has however its own application domain where some factors are preferable over others. The application of each configuration is discussed as follows:

Standard Maximal reduction of line width through the placement of the laser at the top. Very sharp laser line as long as there are not large height differences in the material to be observed. To gain resolution the camera should be placed at a shallow angle at

the cost of camera focus. A shallow angle also introduces inclusion problems and could lead to reflection.

Reverse Perfect focus of the camera on the whole field of view. If the material has large height differences this is however compromised. The laser angle has the same properties as the Standard configuration.

Specular The camera and the laser at a 90 degree angle relative to each other for perfect resolution. Reflection could however introduce problems. Focus and line spreading are also not optimal.

Look-Away Best possible reduction of inclusion and reflection. Very bad resolution.

Our application is on the printing of deposition lines to build parts for additive manufacturing. The lines printed should eventually be controlled to have a constant geometry at all times. Our configuration should be focused on the ability to measure as accurately as possible. A constant surface is extra beneficial for the camera to focus on the entire field of view. Therefore the **Reverse configuration is chosen** as the setup for the vision system.

2.3 Camera

The camera ultimately determines the performance of the system. The performance of the algorithm designed to process images relies on the quality and amount of data per unit of movement of the deposition. Image quality is affected by camera resolution and the amount of data per pixel. A high resolution with a high range of possible values for each pixel amount for maximum variability and best image quality. The amount of data per unit is affected by the optical zoom and the frame rate of the camera. A large optical zoom results in a high amount of pixels per area. A high frame rate results in more measurements.

Low-cost cameras compromise on the above quality aspects. The camera used for this research is a Dino-Lite Camera as shown in Figure 2.3. Important specifications are given in Table 2.3.



Figure 2.4: Dino-Lite Camera

Model	AM7515MZTL Edge
Interface	USB 2.0
Resolution	5MP (2592x1944)
Frame Rate	10fps @ 5MP
Pixel	3-Channel 8-bit RGB
Magnification	10x - 140x Optical
Dimension	10.5cm (H) x 3.2cm (D)

Table 2.2: Dino-Lite Specifications

The Dino-Lite produces 5 Megapixel images at a maximum frame rate of 10 frames per second. The optical zoom is 140 times which makes up for the lower resolution in terms of pixels per area. The frame rate is very low and use for **real-time control is not recommended with this camera**. The camera could miss a corner and for

control purposes a high frame rate is preferred. The quality of the images is however good. This camera is therefore perfectly applicable to measure depositions if time is not a constraint. Off-line use to measure the deposition is possible. Identifying dynamics is hard due to the lack of timed data. **Steady-state modelling is however possible.** The amount of data the camera produces is given in Table 2.3. This amount of data

Pixels/Image	$2.592 * 1.944 = 5.038.848$
Integers/Image	$2.592 * 1.944 * 3 = 15.116.544$
MB/Image	≈ 15
Possible Values/Pixel	$256^3 = 16.777.216$

Table 2.3: Dino-Lite camera data output.

needs however to be processed by the detection algorithm. Expensive hardware and optimized software make it possible to process the data fast. Implementing complex detection algorithms compromise the speed of execution but could improve accuracy of measurement. Simpler algorithms tend to be fast but not as accurate. There has to be found a balance between speed and accuracy of the algorithm. For real-time control purposes high sampling rates could be preferred over super accurate measurement. Furthermore, complex undeterministic algorithms introduce jitter in the sampling rate, which is highly undesirable in control. Since the ultimate goal is real-time control of the deposition geometry **this research focusses on the development of a detection algorithm utilizing simple deterministic image processing methods.**

2.4 Laser-Diode

The laser is used for illumination of the geometry of the object being detected. The lens within the laser converts the dot shaped light to a line. This line has a width which should be relatively small compared to the field of view of the camera, otherwise the whole image the camera produces should be enlightened and it would be impossible to detect geometry. The line could have different intensity profiles. A linear profile has equal intensity along the line. Gaussian lines have intensity according to a gaussian profile, meaning high intensity in the middle and lower at the ends. The output power of the laser is another indicator for overall intensity of the light the laser emits. Different wavelengths produce different colors and have their own advantages with respect to visibility on certain surfaces.



Figure 2.5: Infiniter Line-Laser

Model	VLM-650-30
Interface	Lead Wires
Operating Voltage	5 Volt
Output Power	5mW
Wavelength	650 nm
Fan Angle	60 degree
Line Profile	Gaussian Line
Line Thinkness	< 1.2mm
Accuracy	<1.6mm @ 400mm

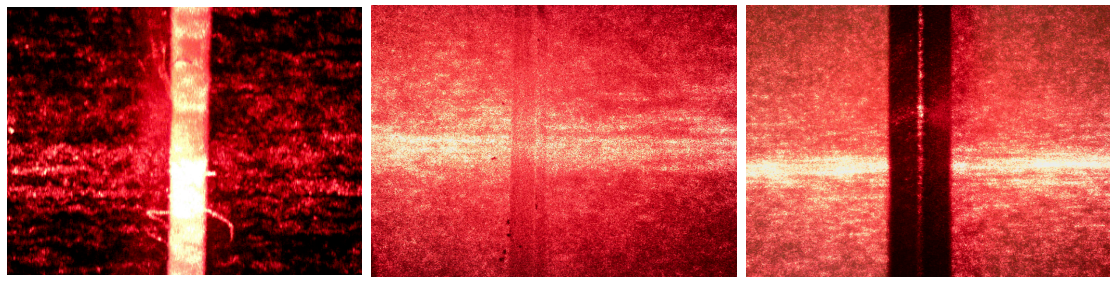
Table 2.4: Laser Specifications.

Low-cost line-lasers compromise on the above quality aspects. The laser used for this research is a Infiniter line laser as shown in Figure 2.4. Important specifications are given in Table 2.4.

The laser produces red light at 650nm and the output power is 5mW. The output power is low and there are no safety restrictions. The line is relatively thick which only allows for proportional large field of view and therefore might restrict the amount of optical zoom used.

2.5 Deposition Material

The material used for printing has a big influence on the image quality produced by the camera. Light reflection can cause pixel saturation which makes detecting differences between the pixels hard or even impossible. Absorption leads to the same problem implied by the lack of light. A material that does not reflect or absorb and passes through makes it impossible to detect differences between the bed and the object to be detected. Figure 2.6 shows the images acquired for different materials. Figure 2.6a



¹For a general discussion of the difference between the *feel* and *think* models of decision making, see H. R. Hershatter, *Decision Making: The *Feel* Model* (New York: Harper & Row, 1969).

shows a white silicon based deposition material which is highly reflective. Contrast between the bed and the deposition is high but saturation of pixels occurs on top of the deposition. Figure 2.6b shows the result for a transparent silicon. Pixels do not saturate but contrast is low. Figure 2.6c shows the image when a black rod is used for material. This rod absorbs most of the light and the laser line does not expose the geometry of the rod.

Due to the reasons explained above this research is focussed on the usage of **white silicon as the deposition material**. The reflection of the material is a disadvantage but could also be the result when a different triangulation configuration was used like the Specular configuration as can be seen in Figure 2.3a. Transparency and absorption make measurement through a triangulation based setup very hard.

3 Algorithm Design Limitations

This chapter analyzes the implied limitations by the data generated and the used algorithmic methods in literature for geometry feature extraction. These limitations will be used to from a new algorithm based upon methods solving the issues at hand.

First the goal of the new proposed algorithm is set. Next, the limitations of the data output from the vision system as described in Chapter 2 are discussed. Followed by a literature review on the previous work done on feature extraction based on laser vision with a discussion on the limitations of the used methods.

3.1 Objective

The goal of the image processing algorithm is to detect deposition feature height and width. The experimental hardware setup used for design of this algorithm is as follows where results from Chapter 2 are used.

- **Reverse Configuration** This triangulation configuration is used for analysis and development of the algorithm.
- **Reflective Material** To make it possible to detect difference between the deposition and the bed a reflective white silicon based material is used as deposition.
- **Low-Quality Hardware** To test for robustness against suboptimal conditions low-quality hardware as in the camera and line-laser are used.

The following subgoals are set for the algorithm design which are focused towards the application of real-time control of the deposition geometry.

- **Fast Mathematical Operations** With real-time control purposes in mind the focus is to use simple mathematical image processing methods to allow for high frame rates.
- **Deterministic Behavior** To keep the amount of jitter acceptable, iterative mathematical operations should be avoided.
- **Robustness** The algorithm should be robust against noise and changing conditions.
- **Flexibility** The influence of different image signatures due to the use of other hardware should be minimized as much as possible.
- **Automated** It should be avoided to use algorithms which demand settings. Hard-coded constants should be avoided as much as possible.

3.2 Data limitations

To achieve robustness against the suboptimal conditions the data generated by the camera is analyzed to identify the effect of the low-quality components on the images created. A typical image from the camera is shown in Figure 3.1 where the laser is positioned at the bottom of the image. The image shows little similarity with the predicted output as in Figure 2.3b. The line is supposed to accurately follow the geometry of the deposition such that it can be used to measure width and height.

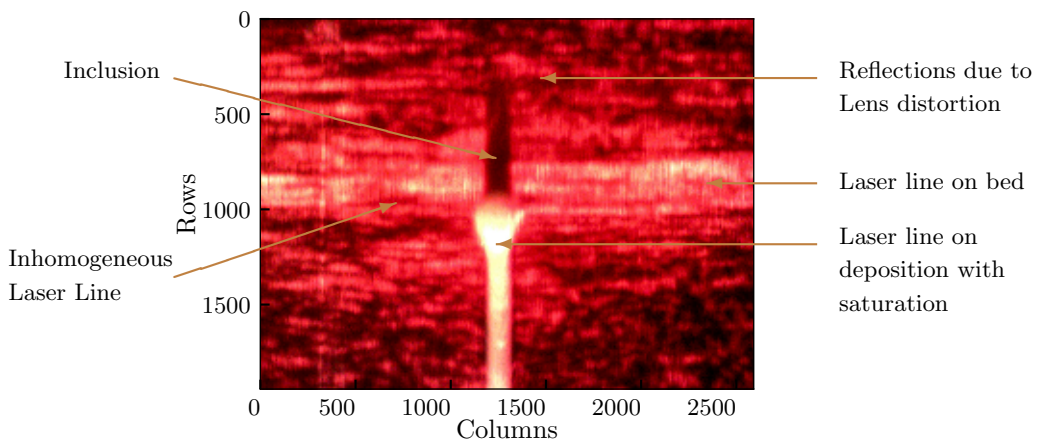


Figure 3.1: Image from vision system with applicable terms to image sections.

Around the laser line are scattered reflections visible. A perfect laser should focus all light to a single line. The laser module is thought to be the source of this artifact. The lens in front of the laser beam converts the shape from a dot to a line. If there are any distortions/inhomogeneities in or impurities on the lens this could result in a scattered line laser beam. Figure 3.1 shows **inhomogeneity in the laser line and reflections of light at unwanted places**. Since the laser will be operating in environments with heat and plastic materials it is possible that the lens gets contaminated.

Reflections onto the print bed which do not belong to the real laser line have made it harder for the algorithm to detect where their separation lays. Identifying whether the reflections on the deposition are generated by the unwanted reflections or by the real laser line is much harder. The bed is a relatively flat surface and the angle of incidence of the light is considered to be about the same across the bed. The deposition is not a flat surface and the angle of incidence differs. As a result **light reflected from the deposition is hard to separate in laser line and light due to lens impurities or distortion**. Furthermore, the **width of the laser line onto the bed can differ from the laser line onto the deposition**. A steep angle for example in the deposition might converge the laser line beam such that it appears smaller on the image.

Next to the reflections there is **saturation of pixels** visible in the image. This problem might be solvable with different hardware for this kind of material with its reflective properties. Another material might however reflect less and pixels would not be illuminated enough by the new hardware. Changing hardware according to the use of different materials is not realistic and the problem should therefore be handled in the detection algorithm.

3.3 Previous Work

To design a new algorithm a literature review is done on image processing for laser triangulation based structured light applications. The process towards extraction of features to be measured differs and many image processing algorithm exist. The general approach for laser triangulation based images can be divided into three stages, image segmentation, line extraction and feature extraction as described in [2]. This literature review summarizes the methods used and points out potential problems of certain methods when applied to the data as shown in Figure 3.1.

Image Segmentation

The goal of segmentation is to divide the image into separate parts. To improve computational efficiency it is common to reduce the image to the range-of-interest. Thresholding the image based on gray-scale intensity is often used to separate the structured light from the image background. To reduce disturbances in the image filters are usually applied before the thresholding.

Range-of-Interest A common first step is to reduce the size of the image to the so called range-of-interest (ROI) to reduce computation time. Manual selection of region size and position as in [3] is only effective for detection of static positioned objects. Another paper [4] manually selects the column and/or row size of the ROI while row or column position is determined by the peak of the average column intensity of the image in gray-scale. This allows the object to move around while region size should be approximately constant. An algorithm to find the ROI position in both directions and determine the size automatically is described in [5] where a manual threshold is set to separate back and fore ground. The bounding box is determined by the maximum and minimum positions of the pixels left after thresholding.

Potential Problems:

- *Information Loss*

Reducing the image size ignores potential information left in the sections outside of the ROI. The laser line outside of the region holds information on the laser line position and size for example. **Since inhomogeneity of the laser line and disturbed areas are a problem as discussed in Section 3.2 it is not recommended to conduct all further analyses based upon a ROI to prevent important information loss.**

- *Flexibility*

Gray-scale single channel images are used for determination of the ROI based upon the pixel intensity. Since most images are colored and consist out of three channels a lot of information is lost. As long as images are used where the structured light is clearly separable from the background by gray-scale intensity this is not a problem. Our case however shows a difference in laser reflection on the bed and on the deposition. Usage of different materials might result in different reflections. **To prepare for different deposition materials it is not recommended to choose a ROI based upon gray-scale intensity since the light reflected from the deposition might not only differ in intensity.**

Noise canceling The distinction between the laser line and background regions is often disturbed by noise. Convolution based filtering with different kernel size and shapes are often used. Paper [3] uses a Gaussian shaped kernel of size 7×7 to smooth the image. In [6] a median filter is used where each pixel value is replaced by the median of neighbouring pixels. There are also frequency based filtering methods as applied in [7] and wavelet methods as in [8]. Next to filtering in the spatial domain there are also papers which filter in the time domain. Removing noise by taking the smallest intensity of each pixel from consecutive images is described in [9].

Potential Problems:

- *Information Loss*

Smoothing the image by filtering removes noise and might remove important information on the exact point of separation between the background and the structured light.

- *Parameter Tuning*

Every filter technique requires a choice for either a kernel size, cutoff-frequency or lag window. It is possible to automate the process at the cost of added complexity.

- *Past Data Influence*

Noise removal by averaging the data over consecutive images will smooth out the algorithms measurements over time. **The problems above give reason to avoid filters where possible.**

Laser segmentation For separation between laser line and background thresholding methods based upon gray-scale pixel value are commonly used. One of the simplest methods is described in [6] where a fixed threshold value is determined by inspection of the image histogram. In [4] the threshold value is automatically determined by using the average of the maximum and minimum pixel intensity. A commonly used histogram thresholding method based upon maximizing the variance between the background and foreground is Otsu's method [10]. Also entropy based methods exist such as in [8]. Next to the global thresholding methods described above there also exist local adaptive methods which adjust threshold locally. An image processing library which implements the most used methods for thresholding is described in [11].

Potential Problem:

- *Position Independence*

The threshold value of the local and global methods are only determined by either its neighbouring pixels or all pixels. The purpose of thresholding is to separate background and foreground at the point of separation. **Pixels far from the point of separation between segments are not important. The methods used by the literature do not utilize this property.**

Laser Line Extraction

The goal of line extraction is to convert the segment holding the laser light to a vector of pixel positions representing the laser line.

Line Position The most used method [12] [13] [9] [3] is to set the peak value of the gray-scale intensity of each column or row as the laser line position. Others [14] [5] [6] take the gradient of the segment edges and set the middle as the laser position. There also exist methods based upon morphology and the watershed algorithm as described in [2].

Potential Problem:

- *Gradients*

Gradients are used to determine change. An advantage of this operation is computational efficiency while the disadvantage is that it is sensitive to noise. Taking the derivative of a signal corrupted by noise will magnify the error. **Often peaks are determined from the gradient which is prone to errors if the Signal-To-Noise ratio is very low.**

Line Cleaning Noise makes it often impossible to detect the laser position for a column or row accurately. To account for these inhomogeneities in the laser line interpolation in combination with a moving average filter can be used as described in [4].

Feature Extraction

After line extraction features to be measured are identified. Every application has its own features to detect. A common approach is to label certain points on the laser line as feature points. Dimensions can then be calculated by the difference between those points. The simplest methods [9] [3] rely on taking second derivatives of the laser line and labeling the absolute values as feature points. In [13] the laser line is segmented into small sections connected to each other (feature points) using polygonal fitting. Paper [14] decides if a point is a feature point based upon linguistic rules set by a threshold.

4 Proposed Algorithm

The limitations identified by visual inspection of the data, the potential problems of the methods used by literature and the objective set for the algorithm as described in Chapter 3 are used in this chapter where a new algorithm is proposed able to detect deposition width and height.

First an overview is given of the steps in the new algorithm, followed by an in depth explanation of the methods used for each step.

4.1 Overview

The common procedure in feature extraction from structured light is discussed in 3.3. The new algorithm is structured differently and this chapter is therefore divided into the following sections:

Image representation

The images generated by the vision system are discussed in terms of data and the output as generated by the experimental setup is visualized.

Deposition Segmentation

The area where the deposition is present is detected and boundaries are determined. Template matching and a Triangle based algorithm are used to improve robustness. This way the segment where the laser illuminates the print bed and the deposition segment are separated.

Laser Line Segmentation

After segmentation of print bed and deposition the laser line on the print bed is segmented from the background. A new thresholding method is proposed which is able to clarify the laser line edge at the point of segmentation.

Width Extraction

The deposition width is then extracted using the same template matching and triangle based algorithm as before. A smaller area is used to allow for local width measurement of the deposition at the edge of the laser line.

Height Extraction

The laser line is segmented from background reflections on the deposition utilizing the same method as used for separation of the laser line on the bed. The height is then determined by measuring the difference in pixels between the edge of the laser line on the bed and the edge on the deposition.

4.2 Image representation

Each image I is represented as a matrix with R rows, C columns and L layers or channels:

$$I \in \mathbb{Z}^{R \times C \times L} \quad (4.1)$$

Values within the image can be represented by the following values where the subscripts r, c, l are used for access to a pixel value:

$$I_{rcl} \in S_0 \quad (4.2)$$

where the pixel values lie within the set:

$$S_0 = \{I_{rcl} \in \mathbb{Z} \mid 0 \leq I_{rcl} \leq 255\} \quad (4.3)$$

Graphical representations of the data generated by the vision system are shown in Figure 4.1. The combined channels are shown in the red-green-blue (RGB) colorspace. The other channels are represented in gray-scale where the value 255 is white and 0 is black. A difference in intensity between channels is visible as I_{rc1} is much brighter than the others.

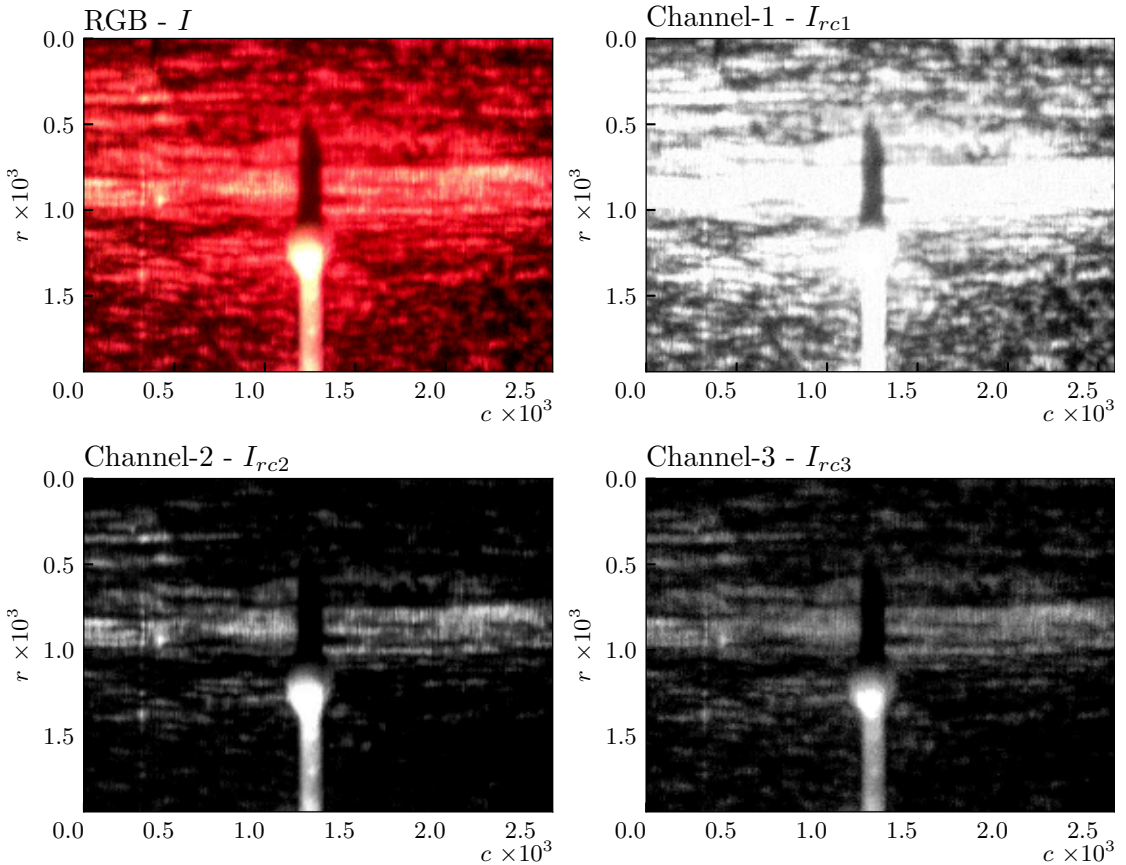


Figure 4.1: Image channels in gray-scale and total image in RGB.

4.3 Deposition Segmentation

To segment the laser line from the background the deposition is separated from the bed first. The algorithm used for segmentation of the laser line, as explained in Section 4.4, would otherwise be disturbed.

Template matching

Segmentation through intensity search is restrictive as explained in 4.4. The sum of pixel values along an axis is the only measure used which ignores difference in distribution or pixel position. Although this approach works for segmentation of laser line and print bed this is not possible for deposition segmentation. Figure 2.3b shows an ideal image of structured light by triangulation. The sum or distribution of the pixel values along the columns are the same. Position of pixel values is the only measure able to detect where the deposition is.

Template matching is therefore used which is able to detect difference in position and distribution. Segmenting the deposition from the bed is only possible if the bed is visible in the image. The sides of the image therefore have to belong to the bed and can be used as a template. The template is defined as follows where the influence of noise is reduced by taking the mean of δ_1 columns from the left and $C - \delta_2$ columns from the right side of the image I .

$$T_{rl} = \frac{1}{\delta_1 + C - \delta_2} \sum_{c \in S_2} I_{rcl}, \quad \forall (r, l) \in S_1 \quad (4.4)$$

where

$$S_1 = \{(r, l) \in \mathbb{Z} \times \mathbb{Z} \mid 1 \leq r \leq R \wedge 1 \leq l \leq L\} \quad (4.5)$$

$$S_2 = \{c \in \mathbb{Z} \mid 1 \leq c \leq \delta_1 \vee \delta_2 \leq c \leq C\} \quad (4.6)$$

Two common methods for matching are cross-correlation and sum-of-squares. Normalized versions of these methods, as described in [15], reduce influence of local intensity variations. Since it is assumed that the intensity of pixels on the bed are very similar to each other and that pixels representing the deposition could be different, normalization is omitted. Furthermore, disturbances could make it impossible to differentiate between deposition and disturbance after normalization. Although both methods show good results the execution of the sum-of-squares method is computational more efficient. The squared error at each pixel position is defined as:

$$SE_{rcl} = (I_{rcl} - T_{rl})^2, \quad \forall (r, c, l) \in S_3 \quad (4.7)$$

where

$$S_3 = \{(r, c, l) \in \mathbb{Z} \times \mathbb{Z} \times \mathbb{Z} \mid 1 \leq r \leq R \wedge 1 \leq c \leq C \wedge 1 \leq l \leq L\} \quad (4.8)$$

and the sum-of-squared error for every columns is:

$$SSE_{cl} = \sum_{r=1}^R SE_{rcl} \quad \forall (c, l) \in S_4 \quad (4.9)$$

where

$$S_4 = \{(c, l) \in \mathbb{Z} \times \mathbb{Z} \mid 1 \leq c \leq C \wedge 1 \leq l \leq L\} \quad (4.10)$$

Figure 4.2 shows the second channel I_{rc2} of the image I in gray-scale, the template T_{r2} , the squared errors SE_{rc2} and the sum of squared errors SSE_{c2} of an image generated by the vision system. A figure can be made for every channel of the image. The position of the large peak in SSE_{c2} represents the deposition. δ_1 and $C - \delta_2$ are both set to 130 as an initial setting which in total is approximately 10% of the total width $C = 2592$.

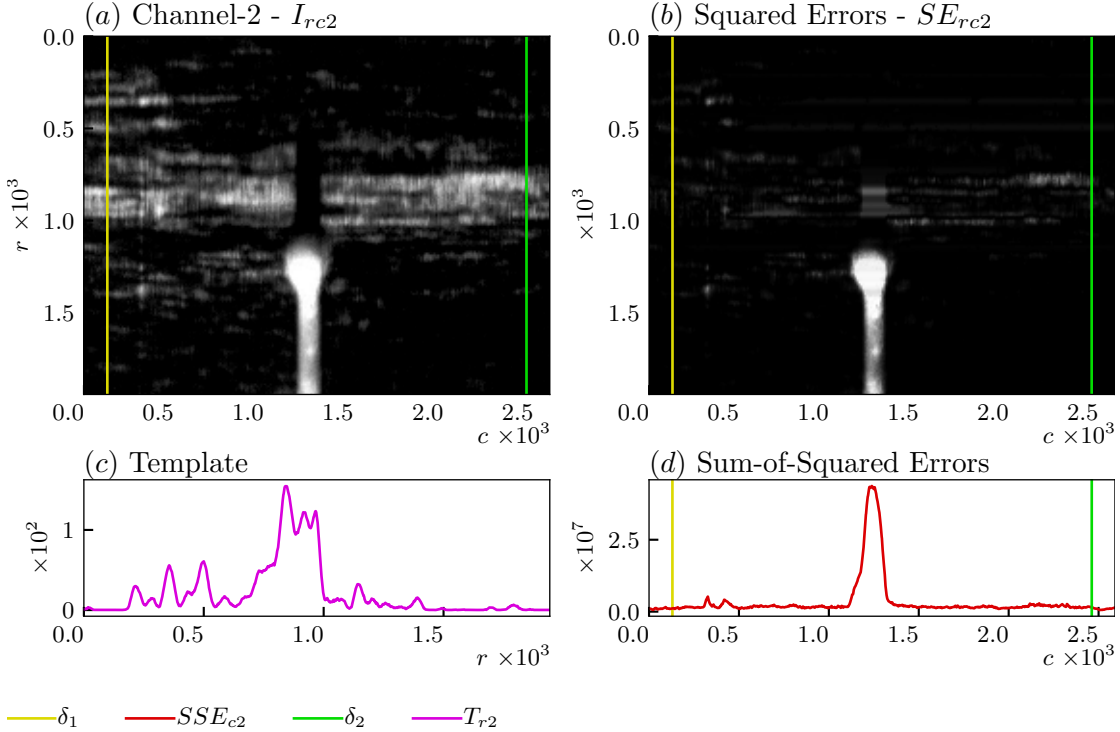


Figure 4.2: Template Matching of I_{rc2} with $\delta_1 = C - \delta_2 = 130$.

Normalization

The sum of squared column errors for each layer are shown in Figure 4.3b. Although the errors seem high for SSE_{c1} they are relatively small compared to the errors of the columns used for calculation of the template. The sum of squared errors are in fact the variance of the column around the template. Before combining the errors of each layer into a total error they are normalized to unit variance. Each error is divided by the mean of the variance M_l of the columns used for the template for each layer.

$$M_l = \frac{1}{\delta_1 + \delta_2} \sum_{c \in S_2} SSE_{cl}, \quad \forall l \in S_5 \quad (4.11)$$

where

$$S_5 = \{l \in \mathbb{Z} \mid 1 \leq l \leq L\} \quad (4.12)$$

The normalized versions $NSSE_{cl}$ as shown in Figure 4.3c of the errors then become:

$$NSSE_{cl} = \frac{SSE_{cl}}{M_l} \quad \forall (c, l) \in S_4 \quad (4.13)$$

The total error is then calculated as the euclidean distance between the layers as follows:

$$TE_c = \sqrt{\sum_{l \in S_5} NSSE_{cl}} \quad \forall c \in S_6 \quad (4.14)$$

where

$$S_6 = \{c \in \mathbb{Z} \mid 1 \leq c \leq C\} \quad (4.15)$$

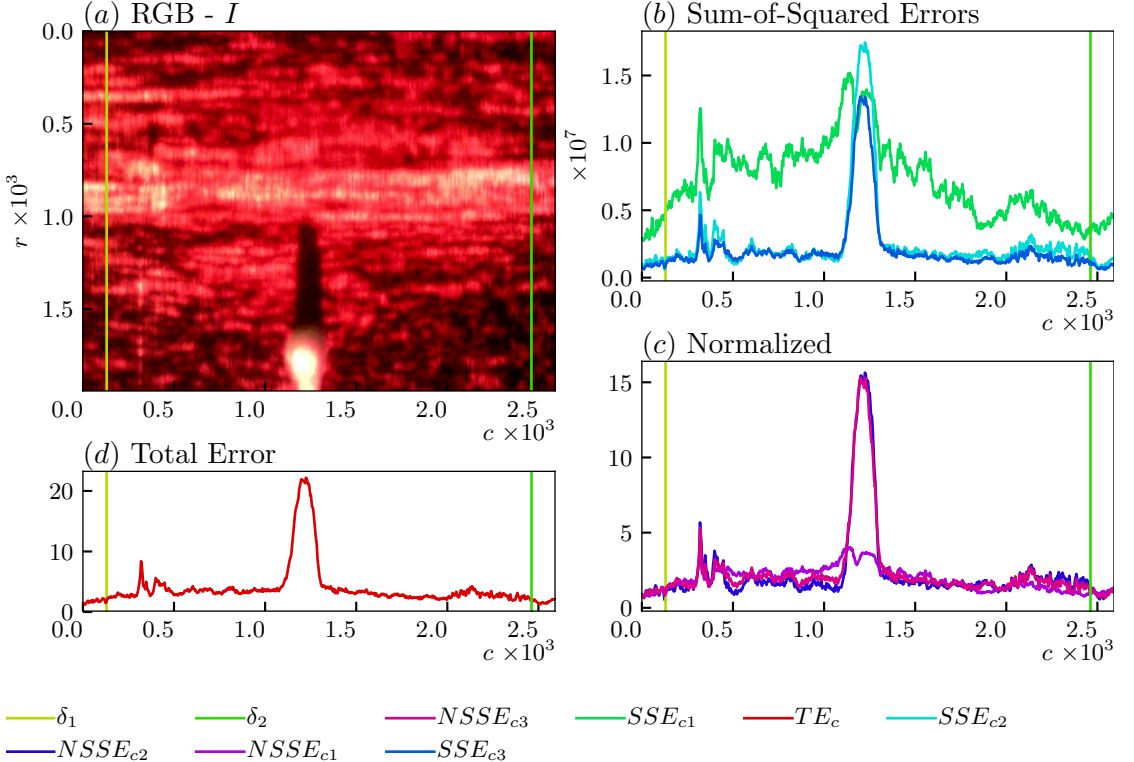


Figure 4.3: Total Error as euclidean distance of normalized sum-of-squared errors.

Segmentation

The total error TE_c is used to separate the deposition from the print bed. Differencing the total error $TE_c - TE_{c-1}$ $\forall c \in S_6$ and calculating the maximum and minimum as the separation points is error prone as shown in Figure 4.4b. The signal-to-noise ratio is low and a filter should have been applied to filter the noise. This is however not preferred as discussed in Section 3.3. Furthermore, calculating the extrema of the differenced series results in finding the points where the total error changes the most. It does however not find the points where the deposition starts. Figure 4.4a shows the image in RGB with δ_1^{DIFF} and δ_2^{DIFF} as the points of separation. A small part of the deposition is much wider than the rest which the method based on differencing does not detect.

The Triangle algorithm as described in [16] is used as a global thresholding method. This method is adapted to serve as a better alternative to separation based on differencing. The first step is to form the piecewise triangle function T_c as follows. The result

is shown in Figure 4.4c.

$$T_c = \begin{cases} TE^{MN}, & \forall c \in S_2 \\ \frac{c-\delta_1}{TE^{AMAX}-\delta_1} (TE^{MAX} - TE^{MN}), & \forall c \in S_7 \\ \frac{\delta_2-c}{\delta_2-TE^{AMAX}} (TE^{MAX} - TE^{MN}), & \forall c \in S_8 \end{cases} \quad (4.16)$$

where

$$S_7 = \{c \in \mathbb{Z} \mid \delta_1 \leq c \leq TE^{AMAX}\} \quad (4.17)$$

$$S_8 = \{c \in \mathbb{Z} \mid TE^{AMAX} \leq c \leq \delta_2\} \quad (4.18)$$

and

$$TE^{MN} = \frac{1}{\delta_1 + C - \delta_2} \sum_{c \in S_2} TE_c \quad (4.19)$$

$$TE^{MAX} = \{TE_{c'} \mid TE_{c'} > TE_c \quad \forall c \in S_6\} \quad (4.20)$$

$$TE^{AMAX} = \{c \mid TE_c = TE^{MAX}\} \quad (4.21)$$

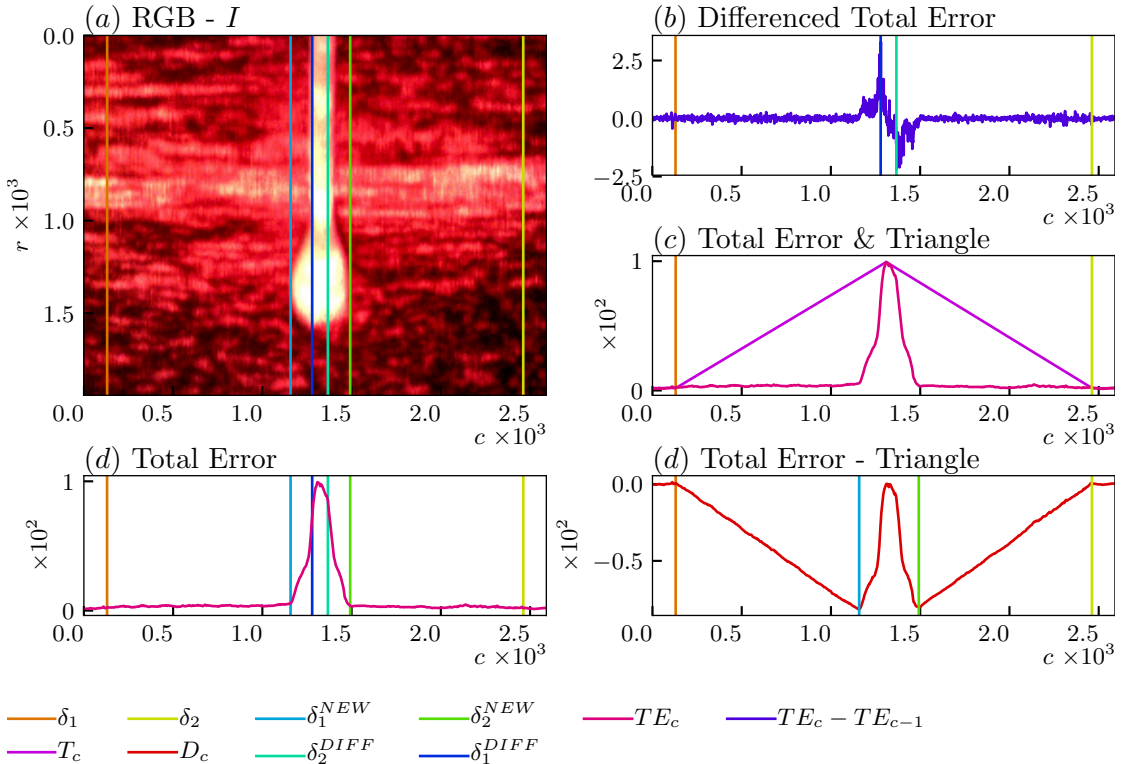


Figure 4.4: Triangle based segmentation versus differencing.

The points of separation δ_1^{NEW} and δ_2^{NEW} are then found by calculating the minima of the difference as follows:

$$\delta_1^{NEW} = \{c \mid D_c = D_1^{MIN}\} \quad (4.22)$$

$$\delta_2^{NEW} = \{c \mid D_c = D_2^{MIN}\} \quad (4.23)$$

where

$$D_c = TE_c - T_c \quad \forall c \in S_6 \quad (4.24)$$

$$D_1^{MIN} = \{D_{c'} \mid D_{c'} < D_c \quad \forall c \in S_7\} \quad (4.25)$$

$$D_2^{MIN} = \{D_{c'} \mid D_{c'} < D_c \quad \forall c \in S_8\} \quad (4.26)$$

The results as shown in Figure 4.4a show that the triangle based method is more sensitive to deposition change than the differencing based method. δ_1^{NEW} and δ_2^{NEW} completely separate the deposition from the bed. The signal-to-noise ratio is very high which improves robustness. Furthermore, there are no parameters to be tuned as no filter is used.

4.4 Laser Line Edge Segmentation

After segmentation of the deposition from the bed it is possible to segment the laser line from the bed. The line position serves as a reference point for height measurement. Furthermore, the width of the deposition is determinant at the position of the laser.

Thresholding

Laser line position is usually determinant by detecting the peak gray-scale intensity value of each column. There are however data implied problems as described in Section 3.2. Saturation of pixels makes peak detection unreliable and inhomogeneity in the line makes column wise detections hard. Width measurement of the line and taking the middle of the line as a reference point is of no use since the width of the laser line onto the bed might be different.

Therefore a single edge is used as reference point and the mean of the row pixels is used as the intensity value. Using the image in gray-scale instead of all layers relies on the assumption that the laser line brightness is highest in the center of the line and is lower the further away from the middle. The image in gray-scale is shown in Figure 4.5a and is calculated by:

$$I_{rc}^{gray} = 0.299I_{rc1} + 0.587I_{rc2} + 0.114I_{rc3}, \quad \forall (r, c) \in S_9 \quad (4.27)$$

where:

$$S_9 = \{(r, c) \in \mathbb{Z} \times \mathbb{Z} \mid 1 \leq r \leq R \wedge 1 \leq c \leq C\} \quad (4.28)$$

The mean of the pixels in each row not belonging to the deposition is shown in Figure 4.5b and is given by:

$$M_{r0} = \frac{1}{\delta_1^{NEW} + R - \delta_2^{NEW}} \sum_{c \in S_{10}} I_{rc}^{gray}, \quad \forall r \in S_{11} \quad (4.29)$$

where:

$$S_{10} = \{c \in \mathbb{Z} \mid 1 \leq c \leq \delta_1^{NEW} \vee \delta_2^{NEW} \leq c \leq C\} \quad (4.30)$$

$$S_{11} = \{r \in \mathbb{Z} \mid 1 \leq r \leq R\} \quad (4.31)$$

Using the Triangle algorithm as described in Section 4.3 to determine the segment where the edge is positioned is possible but very unreliable due to the amount of background noise in the image. Therefore thresholding is used to separate background from

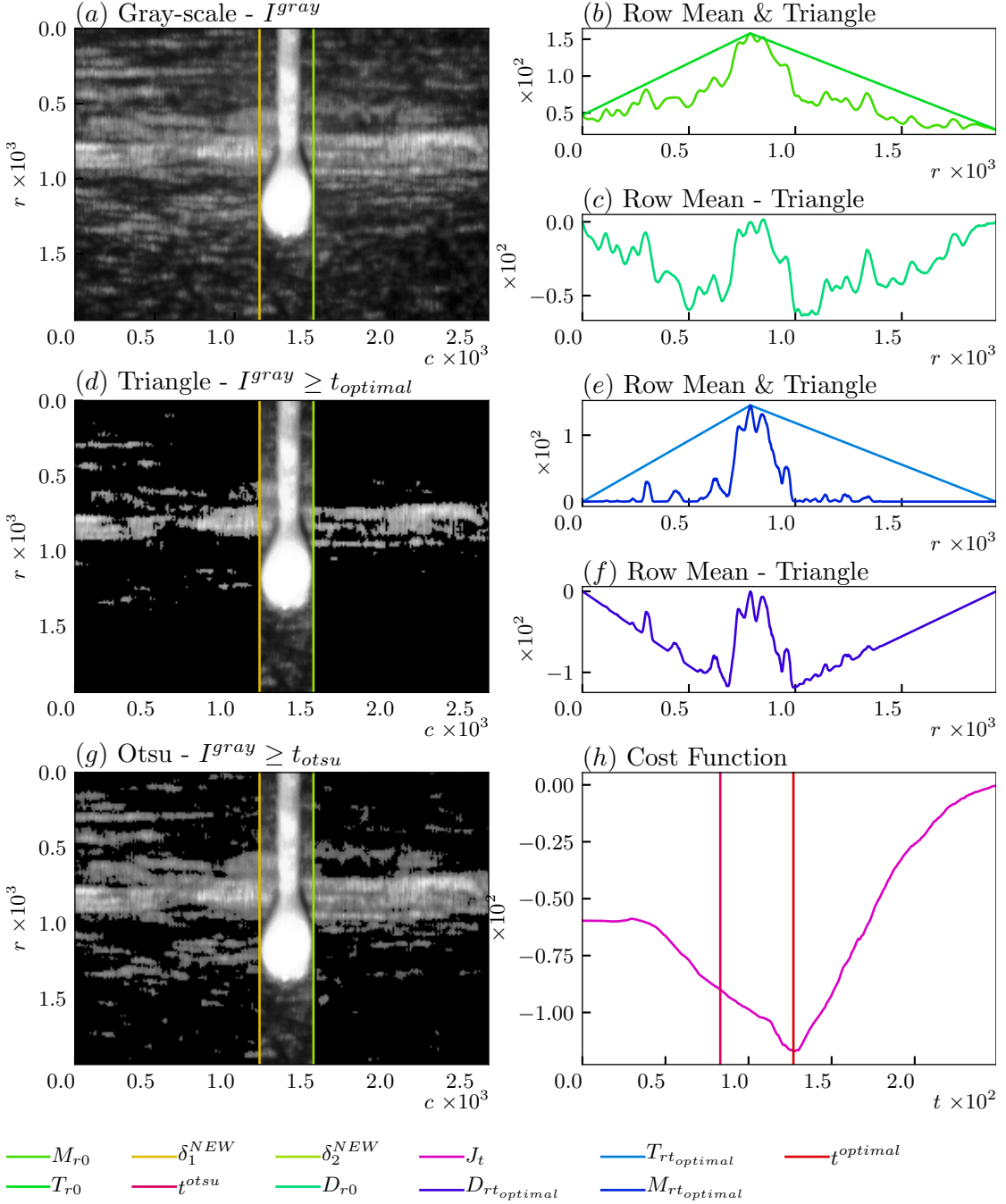


Figure 4.5: Triangle based thresholding versus Otsu's method.

foreground. Otsu's method as described in [10] is one the most used histogram based thresholding methods and the result of this method is shown in Figure 4.5g. Although it does a reseanable job seperating the background from the foreground the algorithm is not focused at clarifying the edge.

A new thresholding method based upon the triangle algorithm is therefore proposed. This algorithm maximizes the distance between the maximum value of the row mean and the value at the position determinant by the triangle algorithm as the edge. The

optimal threshold value is found by:

$$t_{optimal} = \operatorname{argmin}_t J_t, \quad \forall t \in S_0 \quad (4.32)$$

where J_t is the cost function given by:

$$J_t = \min_r D_{rt}, \quad \forall r \in S_{12} \quad (4.33)$$

with:

$$S_{12} = \{r \in \mathbb{Z} \mid 1 \leq r \leq \operatorname{argmax}_r M_{rt}\} \quad (4.34)$$

where D_{rt} is defined as the difference between the mean row intensity M_{rt} at a certain threshold t and T_{rt} is the triangle calculated as before in Section 4.3. The upper edge of the laser line is chosen as reference point. Therefore the cost function is focused at minimizing D_{rt} for all rows before the place where the maximum row intensity $\operatorname{argmax}_r M_{rt}$ occurs.

$$D_{rt} = M_{rt} - T_{rt} \quad (4.35)$$

The mean row intensity M_{rt} is given by:

$$M_{rt} = \frac{1}{\delta_1^{NEW} + C - \delta_2^{NEW}} \sum_{c \in S_{10}} I_{rc}^{gray}, \quad \forall (r, I_{rc}^{gray}, t) \in S_{13} \quad (4.36)$$

where:

$$S_{13} = \{(r, I_{rc}^{gray}, t) \in \mathbb{Z} \times \mathbb{Z} \times \mathbb{Z} \mid 1 \leq r \leq R \wedge I_{rc}^{gray} \geq t \wedge 0 \leq t \leq 255\} \quad (4.37)$$

The cost function J_t at every threshold value is calculated and is displayed in Figure 4.5h. The threshold t^{otsu} is the value as determined by Otsu's method and is clearly sub-optimal in maximizing the difference in mean row intensity between rows at the edge. The optimal threshold as determined by the new algorithm is shown as $t_{optimal}$. The row mean $M_{rt_{optimal}}$ and triangle $T_{rt_{optimal}}$ created for this threshold are shown in Figure 4.5ef and the thresholded image $I^{gray} > t_{optimal}$ is shown in Figure 4.5d.

Segmentation

After thresholding, the rows containing the edge are segmented. Figure 4.6 shows the image in RGB and Gray-scale with the section containing the edge as the rows between δ_3 and δ_4 which are defined as:

$$\delta_3 = \operatorname{argmin}_r D_{rt}, \quad \forall r \in S_{12} \quad (4.38)$$

$$\delta_4 = \operatorname{argmax}_r M_{rt_{optimal}}, \quad \forall r \in S_{11} \quad (4.39)$$

These rows will be used for width extraction. The row at which the edge actual is positioned is defined as the row δ_5 at which the mean pixel value lies exactly in the middle of the mean pixel values of the rows δ_3 and δ_4 . The peak value of the differenced series could also be used but is sensitive to noise and requires filtering which is not preferred.

$$\delta_5 = \{r \mid M_{rt_{optimal}} = (M_{\delta_4 t_{optimal}} - M_{\delta_3 t_{optimal}}) / 2\} \quad (4.40)$$

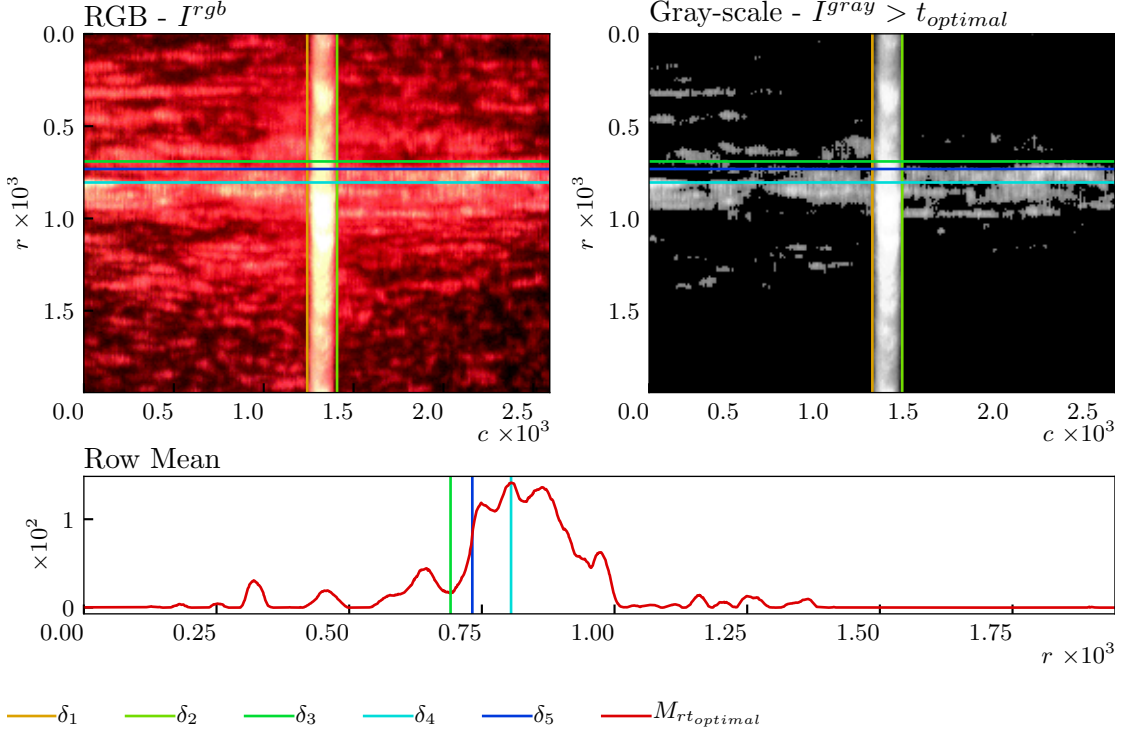


Figure 4.6: Edge segmentation of the laser line on the print bed.

4.5 Width measurement

The rows containing the laser line edge, $\delta_3 \leq r \leq \delta_4$, are used to determine the width of the deposition at the edge. A single row could be used for width determination depending on the amount of disturbance in the laser line. If there was a clear distinction between laser line and background then δ_3 and δ_4 would be closer to each other. A perfect laser line without disturbance would result in $\delta_4 = \delta_3 + 1$.

The width is determined using the same template matching method as described in Subsection 4.3. The columns used for forming the template are all columns S_{10} belonging to the bed. The template is formed according to:

$$T_{rl} = \frac{1}{\delta_1^{NEW} + C - \delta_2^{NEW}} \sum_{c \in S_{10}} I_{rcl}, \quad \forall (r, l) \in S_1 \quad (4.41)$$

The normalized errors for each layer and the total error are determined according to Subsection 4.3. The Triangle algorithm is applied to find the edges δ_7 and δ_8 of the deposition at the rows which include the laser line edge δ_5 . The result is shown in Figure 4.7. The width W of the deposition is then calculated by:

$$W = \delta_7 - \delta_6 \quad (4.42)$$

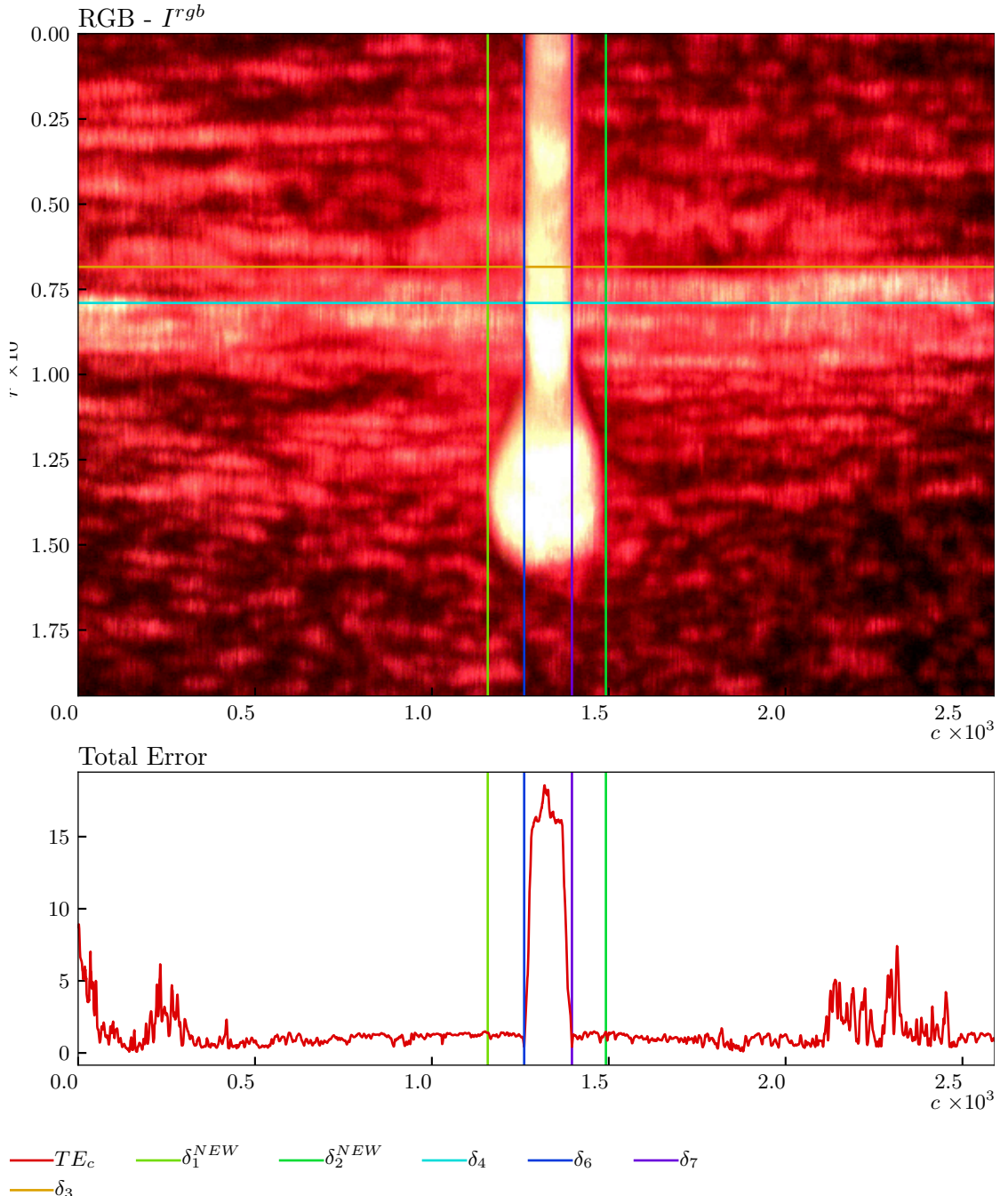


Figure 4.7: Width extraction at the position of the laser line edge.

4.6 Height measurement

To measure deposition height H , the difference between the laser line edge on the bed δ_5 and the edge on the deposition δ_{10} is calculated. The actual height can be calculated from the angle of the laser relative to the bed.

$$H = \delta_{10} - \delta_5 \quad (4.43)$$

The results of all algorithms needed for height extraction are shown in Figure 4.8. The bed, which are all columns c in S_{10} , is globally thresholded with threshold $t_{optimal}^{BED}$ using

the Triangle threshold method as described in Section 4.4. The columns representing the deposition $\delta_6 \leq c \leq \delta_7$ are thresholded utilizing the same method with $t_{optimal}^{DEPOSITION}$ as a result. The row means after the application of these thresholds are displayed as $M_{rt_{optimal}}^{BED}$ for the bed and $M_{rt_{optimal}}^{DEPOSITION}$ for the deposition.

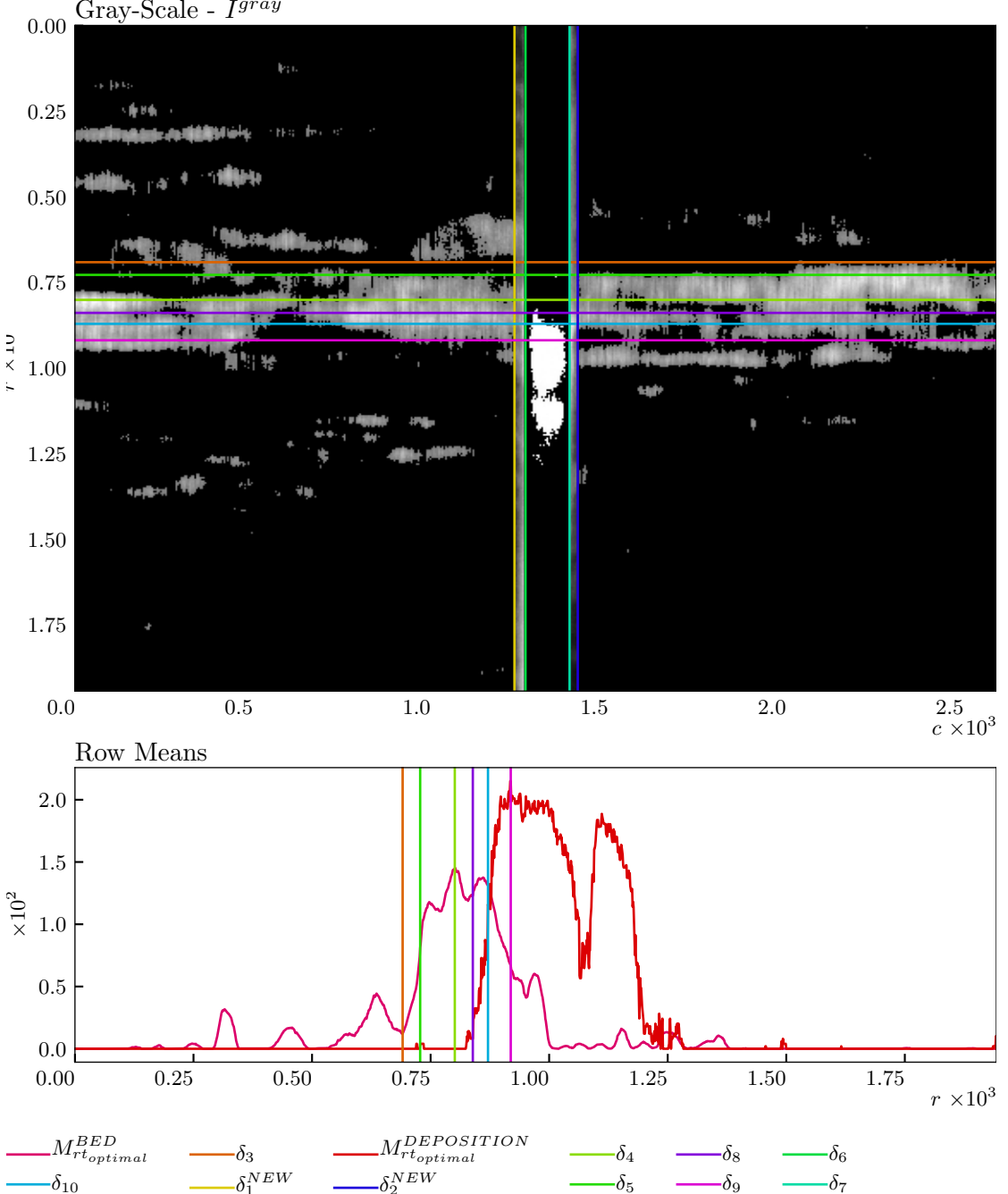


Figure 4.8: Height extraction.

5 Conclusions and Recommendations

The main goal was to develop a robust vision based algorithm able to detect deposition height and width under sub-optimal hardware induced conditions. Furthermore, the algorithm should be flexible and applicable to many different image signatures.

Many algorithms in literature neglect sub-optimal conditions like pixel saturation and laser line inhomogeneity. Most methods rely on peak detection of gray-scale images, edge detection using gradients and filtering to reduce noise.

This research used template matching as a metric to replace gray-scale intensity which improves sensitivity to changes. The Triangle algorithm has been adapted as a replacement to the use of gradients leading to improved robustness against noise and sensitivity to change. Filtering has not been necessary for noise reduction and no parameters are used within the new algorithm except for an initial amount of columns used as template. A new global thresholding method has been developed focused at clarifying the edge with superior performance compared to Otsu's method.

The algorithm is able to detect width and height of deposition material for additive manufacturing processes. It has been tested on a experimental vision system using low-cost hardware. The algorithm works under pixel saturation due to measurement of the laser line edge instead of peak values. Inhomogeneity of the laser line is taken into account by using average row and column pixel values.

Deposition height is measured as an average of all columns covering the deposition. This could in future work be improved to measure height at every column to identify the shape of the deposition. The measurements could also be improved by introducing sub-pixel accuracy.

Bibliography

- [1] Mihaela Vlasea and Ehsan Toyserkani. Experimental characterization and numerical modeling of a micro-syringe deposition system for dispensing sacrificial photopolymers on particulate ceramic substrates. *Journal of Materials Processing Technology*, 213(11):1970–1977, 2013.
- [2] Yuan Li, Qinglin Wang, De Xu, Zhiguo Yan, and Min Tan. Recent developments on welding image processing and features extraction. *Measurement and Control*, 40(5):139–145, 2007.
- [3] Wei Huang and Radovan Kovacevic. Development of a real-time laser-based machine vision system to monitor and control welding processes. *The International Journal of Advanced Manufacturing Technology*, 63(1-4):235–248, 2012.
- [4] Xiuping Wang, Ruilin Bai, and Ziteng Liu. Weld seam detection and feature extraction based on laser vision. In *Control Conference (CCC), 2014 33rd Chinese*, pages 8249–8252. IEEE, 2014.
- [5] De Xu, Zemin Jiang, Linkun Wang, and Min Tan. Features extraction for structured light image of welding seam with arc and splash disturbance. In *Control, Automation, Robotics and Vision Conference, 2004. ICARCV 2004 8th*, volume 3, pages 1559–1563. IEEE, 2004.
- [6] Lei Zhang, Mingyang Zhao, and Lihua Zhao. Vision-based profile generation method of twb for a new automatic laser welding line. In *Automation and Logistics, 2007 IEEE International Conference on*, pages 1658–1663. IEEE, 2007.
- [7] Isa Servan Uzun, Abbes Amira, and Ahmed Bouridane. Fpga implementations of fast fourier transforms for real-time signal and image processing. *IEE Proceedings-Vision, Image and Signal Processing*, 152(3):283–296, 2005.
- [8] Xiwen Liu, Guorong Wang, and Yonghua Shi. Image processing of welding seam based on single-stripe laser vision system. In *Intelligent Systems Design and Applications, 2006. ISDA '06. Sixth International Conference on*, volume 2, pages 463–470. IEEE, 2006.
- [9] Yuan Li, You Fu Li, Qing Lin Wang, De Xu, and Min Tan. Measurement and defect detection of the weld bead based on online vision inspection. *IEEE Transactions on Instrumentation and Measurement*, 59(7):1841–1849, 2010.
- [10] Nobuyuki Otsu. A threshold selection method from gray-level histograms. *IEEE transactions on systems, man, and cybernetics*, 9(1):62–66, 1979.
- [11] Itseez. Open source computer vision library. <https://github.com/itseez/opencv>, 2015.
- [12] Huu-Cuong Nguyen and Byung-Ryong Lee. Laser-vision-based quality inspection system for small-bead laser welding. *International journal of precision engineering and manufacturing*, 15(3):415–423, 2014.

- [13] Jae Seon Kim, Young Tak Son, Hyung Suck Cho, and Kwang Il Koh. A robust method for vision-based seam tracking in robotic arc welding. In *Intelligent Control, 1995., Proceedings of the 1995 IEEE International Symposium on*, pages 363–368. IEEE, 1995.
- [14] Tyler A Davis and Yung C Shin. Vision-based clad height measurement. *Machine Vision and Applications*, 22(1):129–136, 2011.
- [15] MB Hisham, Shahrul Nizam Yaakob, RA A Raof, AB A Nazren, and NM Wafi Embedded. Template matching using sum of squared difference and normalized cross correlation. In *Research and Development (SCOReD), 2015 IEEE Student Conference on*, pages 100–104. IEEE, 2015.
- [16] GW Zack, WE Rogers, and SA Latt. Automatic measurement of sister chromatid exchange frequency. *Journal of Histochemistry & Cytochemistry*, 25(7):741–753, 1977.